Mars Entry, Descent, and Landing Trajectory and Atmosphere Reconstruction

Author:
Soumyo Dutta

Advisor:
Dr. Robert D. Braun

May 5, 2010

Mars Entry, Descent, and Landing Trajectory and Atmosphere Reconstruction

Soumyo Dutta

Georgia Institute of Technology, Atlanta, GA, 30332-1510

Flight data from an entry, descent, and landing (EDL) sequence can be used to reconstruct the vehicle's trajectory as well as compute the associated uncertainty. The atmospheric profile encountered by the vehicle can similarly be estimated from the flight data. Past Mars missions have contained instruments, such as accelerometers, gyroscopes, and radar altimeters that do not provide direct measurement of the free-stream atmospheric conditions. Thus, uncertainties in the atmospheric reconstruction and the aerodynamic database knowledge cannot be separated. However, the upcoming Mars Science Laboratory (MSL) will take measurements of the pressure on the aeroshell forebody during entry. These measurements will provide means to determine the free-stream conditions and to separate the atmospheric and aerodynamic uncertainties. In this paper, analytical methods to statistically estimate trajectories and free-stream conditions from flight data and to quantify uncertainties in these parameters are discussed. A sample data set from a ballistic range test of an Orion Crew Exploration Vehicle (CEV) model is then used to demonstrate results from applying these procedures. This approach utilizes the same techniques and toolset planned for subsequent application for the reconstruction of MSL's EDL sequence in 2012.

Nomenclature

$a_{0,x}, a_{0,y}, a_{0,z}$	Vehicle center of mass acceleration	$\mathbf{x}$	State deviation vector
$\mathbf{A}$	Equation of motion Jacobian matrix	$\mathbf{X}$	State vector
$\mathbf{B}$	State noise Jacobian matrix	$\mathbf{y}$	Observation residual vector
C_A	Axial force coefficient	α	Angle of attack
C_p	Pressure coefficient	β	Sideslip angle
e_0, e_1, e_2, e_3	Quaternions	γ	Flight path angle
$\mathbf{e}$	State error vector	ϵ	Observation error
g	Gravitation acceleration	ζ	Clock angle
h	Altitude	η	Cone angle
H	Observation sensitivity matrix	θ	Pitch angle
$\mathbf{I}$	Moment of inertia	Θ	Longitude
I	Identity matrix	ρ	Density
K	Kalman gain	σ	Standard deviation
m	Vehicle mass	ϕ	Roll angle
M	Mach number	Φ	Planet-centric latitude
p, q, r	Inertial vehicle angular velocity	$\mathbf{\Phi}$	State transition matrix
P	Pressure	ψ	Yaw angle
$\mathbf{P}$	State covariance matrix	Ω	Angular velocity of planet
q	Dynamic pressure		
$\mathbf{Q}$	State noise covariance matrix	*Subscript and superscripts*	
r	Position	b	Backward pass
R	Ideal gas constant	f	Forward pass
$\mathbf{R}$	Observation covariance matrix	i	Pressure port condition
S	Vehicle reference area	k	Time index
T	Temperature	t	Total condition
V	Inertial velocity	∞	Free-stream condition
u, v, w	Inertial velocity components	$-$	Nominal value
$\mathbf{w}$	State noise vector	$\wedge$	Best estimate

I. Introduction

Post-flight reconstruction of the entry, descent, and landing (EDL) sequence has been conducted for every successful Mars mission to provide insight into the vehicle's trajectory and atmospheric conditions it encountered during the descent.[1–4] Previous Mars missions have provided flight data from on-board accelerometers, gyroscopes and radar altimeters, which have allowed estimation of the position, velocity and attitude of the vehicles during the EDL timeline. Moreover, based on the sensed decelerations on the vehicle, the atmospheric profiles encountered by the vehicles have also been estimated.

However, the estimated trajectories and atmosphere from flight data have not reduced the uncertainties in the engineering models used during the design of Martian probes. Particularly, the aerodynamic coefficients of the vehicles have large uncertainties associated with them and that can affect the predicted trajectory. The coefficients in the vehicle aerodynamic database are largely a product of wind-tunnel testing, computational fluid dynamics (CFD) analysis and some Earth-based flight testing. Thus, when the results of the different methods are combined in a database, there exist uncertainties that are inherent in an amalgam of data. Moreover, when the reconstructed aerodynamic coefficients from flight data are compared with the coefficients from the database, discrepancies between the two values can be noticed.[5] In addition, the knowledge Martian atmosphere also contains large uncertainties, which in turn propagate into the uncertainties in the EDL performance of the vehicle. For example, atmospheric models used by NASA during pre-flight trajectory analysis can have 3σ uncertainties as large as $\pm 40\%$ from the nominal value.[6] Thus, Martian EDL reconstructions from flight data can significantly benefit from methods that can estimate and in turn reduce the uncertainties in the design parameters.

Many previous reconstructions[1–4] have used a deterministic process in which the uncertainties of the measurements have not been included directly in the estimation process. If statistical estimation methods are used to reconstruct the trajectory from flight data, the uncertainties in the observations can be incorporated into the estimation process, yielding the associated uncertainty in the reconstructed data.[7] Moreover, in the past, when the reconstructed trajectory has been used to estimate the atmospheric profile, uncertainties in the atmospheric conditions and in the knowledge of the aerodynamic coefficients of the vehicle have not been separable. Primarily, this has been due to a lack of an independent atmospheric measurement source, since most Mars missions have lacked direct atmospheric sensors and have relied largely on inertial measurements; thus, one could not estimate the free-stream conditions of the atmosphere without assuming perfect knowledge of the vehicle aerodynamic database.

Fortunately, the upcoming Mars Science Laboratory (MSL) mission will contain on board pressure transducers that will measure the pressure along the vehicle forebody.[8] Seven pressure transducers located at known locations on the forebody will capture the pressure distribution on the vehicle through the hypersonic phase of entry. The pressure transducers are part of the MSL Entry, Descent, and Landing Instrumentation (MEDLI) project. One of the project's goals under the Mars Entry Atmospheric Data System (MEADS) program is to determine free-stream conditions such as dynamic pressure (q_∞) and Mach number (M_∞), and vehicle orientation parameters, such as angle of attack (α) and sideslip angle (β). The pressure transducer measurements will provide surface pressure measurements independent of the inertial measurements and radar altimeter data, thus allowing a reconstruction of atmospheric parameters independent of the aerodynamic uncertainties.

This paper will present a framework on how to use surface pressure measurements in a trajectory and atmosphere reconstruction that integrates the uncertainties in the data within the estimation process. Past work done in trajectory reconstructions using pressure measurements will be presented, and traditional methods of atmospheric estimation will be analyzed. Subsequently, a reconstruction procedure using an extended Kalman filter (EKF) algorithm will be presented to statistically estimate the trajectory. Modifications necessary to incorporate pressure measurements in the process will also be discussed. Finally, data sets from ballistic range test of the Orion Crew Exploration vehicle (CEV) will be used as a test case for the methodology.

II. Background

Since the landing of Vikings 1 and 2 in 1976, the United States has successfully sent four other spacecrafts to the Martian surface. However, failures have also accompanied the human exploration of Mars, such as the lost 1999 Mars Polar lander mission that lost contact during EDL. Mitigating large uncertainties that exist in engineering models used during Mars EDL design may help avoid some the problems of previous missions. Trajectory and atmospheric reconstruction of flight data allows quantification of the uncertainties in the vehicle performance and the Martian

environment. The following sections will describe the goals behind trajectory and atmospheric estimation from flight data and consider past works done in the field of Mars EDL reconstruction.

A.   Motivation

The objective for the trajectory and atmosphere reconstruction of missions is to verify the performance of the vehicle and quantify any off-nominal behavior. However, this paper's primary focus is to consider methods that can quantify the uncertainties in the estimated trajectory and atmosphere. The effects of these uncertainties in trajectory and atmospheric parameters have to be considered during the design process. Due to a lack of Mars-like testing facilities on Earth, the best substitute is Monte Carlo simulation analysis of the primary design variables. Almost every Mars mission has been simulated using Monte Carlo technique, and results of the analysis can be found in the literature for missions such as the Mars Exploration Rovers (MER)[9] and the Phoenix lander.[10]

Looking at the work of Striepe et al.[11] who conducted a Monte Carlo simulation of the MSL mission, one sees a long list of design parameters with uncertainties to consider. Uncertainties exist in the entry conditions (such as flight path angle), center of mass location of the vehicle and sensor biases that will effect the deployment of a stage in the mission. However, two major sources of uncertainties comes from the lack of certainty in the knowledge of the aerodynamic coefficients of the vehicle and the atmospheric profile it will encounter.

The uncertainties in the aerodynamic coefficients exist due to the various methods used to generate the aerodynamic database for a vehicle. As the work of Edquist et al.[12] shows, the data is compiled from methods such as CFD tools that solve the Navier-Stokes equations, Direct Simulation Monte Carlo Analysis codes that compute aerodynamic effects in the free-molecular regime, bridging models between free-molecular and continuum regimes and ballistic range and wind tunnel data. A sample of the uncertainties in the aerodynamic database for Phoenix is summarized in Table 1.

Due to the various sources that account for the data, the uncertainties are often based on past experience and engineering judgment of the designers. Additionally, aerodynamic data from past missions that are similar to the vehicle being studied are used to complete the aerodynamic database. Since all U.S. Mars missions have used the 70-degree sphere-cone for entry and then used a Disk-gap-band (DGB) parachute, past aerodynamic data is often relevant for future missions. However, despite having flight data from the past missions, the uncertainties have not been significantly reduced.

Table 1. Mars Phoenix aerodynamic uncertainties.[12]

Statics/Dynamics	Flight Regime	Coefficients	3σ Uncertainty	Distribution
Statics	Transitional/Free-Molecular	C_A	$\pm 5\%$	Normal
		C_N, C_Y	± 0.01	
		C_m, C_n	± 0.005 x [1.2 ,0.8]	
Statics	Hypersonic	C_A	$\pm 3\%$	Normal
		C_N, C_Y	± 0.01	
		C_m, C_n	± 0.002 x [1.2 ,0.8]	
		C_l	1.24 x 10^{-6}	
Statics	Supersonic	C_A	$\pm 10\%$	Normal
		C_N, C_Y	± 0.01	
		C_m, C_n	± 0.005 x [1.2 ,0.8]	
		C_l	1.24 x 10^{-6}	
Statics	Transonic	C_A	$\pm 10\%$	Normal
		C_N, C_Y	1.25 x Supersonic	
		C_m, C_n	± 0.005 x [1.2 ,0.8]	
		C_l	1.24 x 10^{-6}	
Dynamics	Hypersonic	C_{mq}, C_{nr}	± 0.15	Normal
Dynamics	Supersonic	C_{mq}, C_{nr}	+ 0.5 x [2.5, 0.5]	Uniform
			- 0.5 + [0.1, 0.0]	
Dynamics	Transonic	C_{mq}, C_{nr}	1.25 x Supersonic	Uniform

Flight data from the two Viking landers provided in-situ atmospheric pressure measurements over the vehicle forebody during EDL. Although the data was not statistically analyzed and uncertainties in the aerodynamic and at-

mospheric properties were not separated, reconstructed angle of attack and lift and drag coefficients histories provided a good benchmark to compare predictions from the aerodynamic database. Edquist's[5] work compares the predictions from LAURA, a CFD tool used to create the aerodynamic databases of several Mars vehicles and the reconstructed flight data. Figure 1 shows the total angle of attack (α_t), lift coefficient, drag coefficient and lift-to-drag ratio for Viking Lander 1 based on CFD tools and flight data. As can be seen in the figure, there are some significant discrepancies between the flight data and the predicted results. These figures underscore the need for using flight data and their reconstructed uncertainties to aid in model verification.

(a) Total Angle of Attack

(b) Lift Coefficient

(c) Drag Coefficient

(d) Lift-to-Drag Ratio
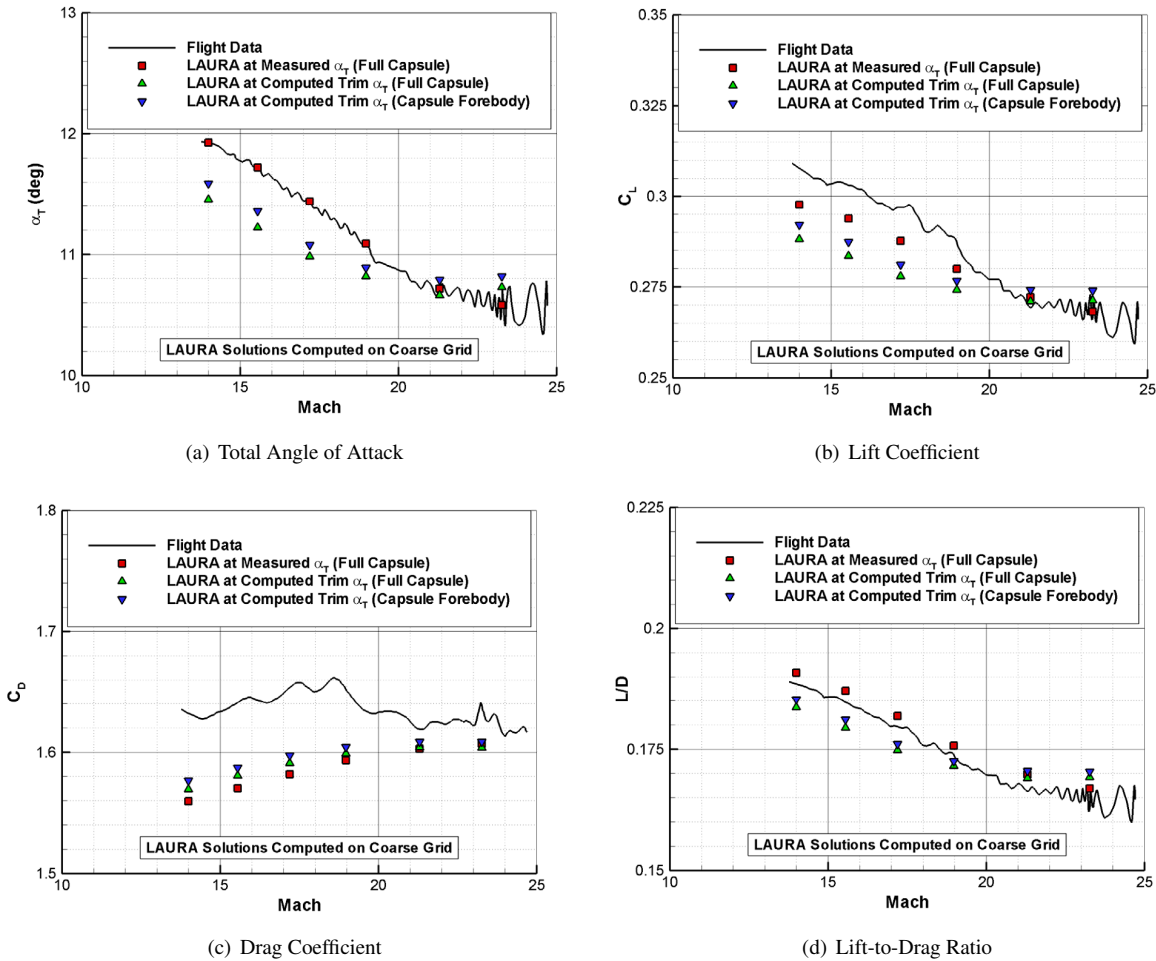
Figure 1. Viking lander 1 aerodynamic coefficients based on flight data and LAURA.[5]

The other significant component of uncertainties in simulations come from atmospheric models. Large variations in the atmosphere due to the seasons, the amount of dust particles and other weather-related events make the prediction of density, pressure and temperature very uncertain. For example, looking at Fig. 2, one can see large variations in density from the nominal prediction.[6] This nominal case is based on the Kass-Schofield model, which was used by Desai et al. to predict atmospheric properties for MER trajectories. Reconstruction of atmosphere from flight data and then quantifying the uncertainties can significantly improve the atmospheric modeling for Mars.

B. Historical Perspective

As mentioned earlier, the United States has successfully landed six spacecrafts on the Martian surface. In addition, MSL is expected to reach Mars in 2012. The past missions have collected various measurements types during EDL that have allowed engineers to reconstruct the trajectory taken and the atmosphere encountered by the spacecrafts. Table 2 summarizes the measurements taken during the EDL phase by the U.S. missions. Table 2 shows that many of the
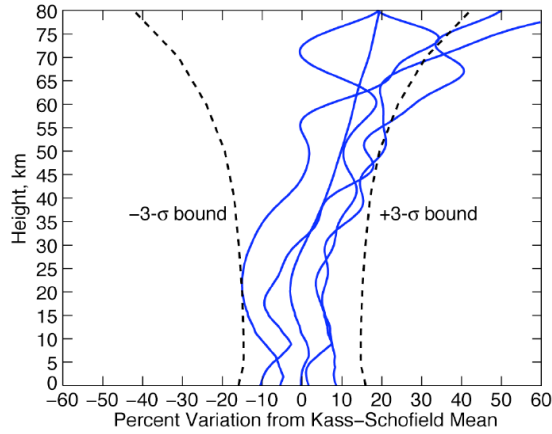
Figure 2. Sample density variation on Mars for MER trajectories. [6]

Table 2. EDL-related measurements taken by U.S. Martian missions.

Measurements	Viking 1 and 2 [4,13]	Pathfinder [1,14,15]	MER [2,16]	Phoenix [3,17]	MSL [8]
Accelerometer	x	x	x	x	x
Thee-axis gyroscope	x		x	x	x
Radar altimeter	x	x	x	x	x
Radiometric tracking (pre-EDL)	x	x	x	x	x
Pressure (during EDL)	x	x			x
Pressure (from surface)	x	x	x	x	x
Temperature (during EDL)	x	x			x
Temperature (from surface)	x	x	x	x	x
TPS Recession					x

past missions have only taken inertial measurement unit and radar altimeter data during the EDL sequence. Thus, the reconstruction techniques for the most part have been limited to deterministic estimation methods. These estimation techniques are similar to methods used to reconstruct data from strap-down guidance systems.[18] The procedure is simply to use the inertial measurements to integrate non-linear equations of motion. Section III. will describe the procedure in greater detail. Results from the deterministic trajectory reconstructions can be found in the literature for Vikings 1 and 2 [4], Mars Pathfinder [1], Mars Exploration Rovers (MER) [2] and the Phoenix lander [3,17].

Moreover, there have been some EDL trajectory reconstruction efforts in the past that have utilized statistical estimation techniques. The method of choice has been the Kalman-Schmidt filter, which is a variant of the more famous Kalman filter. Kalman filtering is a method of estimating parameters when measurements are sequentially processed. This is different from another common estimation technique known as the batch filtering method, which processes all of the data together. Kalman filtering has been applied to flight reconstruction problems as early as the 1970's.[19] Section IV. will describe the algorithm behind a basic Kalman filter, its non-linear variant, the extended Kalman filter, and also describe the modifications needed for a Kalman-Schmidt filter.

In the case of Mars EDL trajectory reconstruction, Kalman filtering was utilized by Euler et al.[13] in 1978 to estimate the trajectories for Viking 1 and 2. Euler integrated the equations of motion using the inertial data, and the used the radar altimeter and the terminal landing Doppler data to correct the estimate of the trajectory parameters through a stochastic filter. Yet, although the Viking probes sampled the atmosphere during EDL using pressure probes, Euler's work did not include the pressure measurements within the trajectory estimation procedure; thus, a statistical estimation of both the trajectory and the atmosphere was not conducted at that point.

Kalman filtering was also used by Spencer et al.[1] in the reconstruction of the Mars Pathfinder data. The tool in this case was a linearized Kalman filter that corrected a nominal trajectory based on the integration of the inertial measurement data. Altimeter and Doppler data were used as measurement types for the Kalman filter. Spencer et al. also utilized a smoothing algorithm to combine trajectory reconstruction from forward and backward runs of the

data. See Section IV. for details regarding the rationale and methodology behind a smoother. However, it is important to note that the Pathfinder reconstruction was conducted using only three degree-of-freedom equations of motion and did not report body-fixed angular rates of the vehicle. The Spencer et al. work also used a least-squares estimator for reconstruction effort in addition to the Kalman filtering reconstruction; thus, that paper has also been cited as an example of deterministic trajectory reconstruction.

Another objective for the Mars flight reconstruction projects through the years has been to determine the atmospheric profile encountered by the vehicles during EDL. Without pressure measurements during EDL, density and other atmospheric properties have been estimated using the knowledge of aerodynamic coefficients and the reconstructed velocity of the vehicle. See Section III. for the deterministic procedure used in the past for atmospheric reconstruction. Deterministic atmospheric reconstruction procedures similar to what is discussed later were proposed as early as 1965 by Seiff and Reese.[20]. Atmospheric reconstructions of Mars missions using deterministic techniques exist in the literature for the Viking missions[21], Mars Pathfinder[1], MER[16] and Phoenix[3].

As noted in Table 2, observations from on-board pressure transducers to estimate the free-stream conditions have been collected previously. Specifically, the two Viking missions and Mars Pathfinder have taken in-situ pressure measurements during the EDL sequence. However, Pathfinder only took the pressure measurements after parachute deployment[14] and thus that data cannot be used to reconstruct the atmosphere during the hypersonic EDL phase. Additionally, Schofield et al.'s work in reconstructing the atmosphere for the Pathfinder mission used the deterministic atmospheric technique described later in this paper.

Viking 1 and 2, on the other hand, did take pressure measurements even in the hypersonic phase of EDL.[21] Nevertheless, the Viking reconstruction also used another deterministic approach in atmospheric reconstruction. Density was calculated using the definition of axial force coefficient (see Eq. (2)) and knowledge of the coefficients from the vehicle aerodynamic database. Then the measurements of the stagnation pressure values during EDL were used to reconstruct the axial force coefficient and an iterative scheme was used to converge on the density values.[22] Thus, the pressure measurements were not directly used in the trajectory estimation and the uncertainties in the pressure measurements were not included in the estimation algorithm.

Nevertheless, flight reconstructions for non-Mars EDL sequences have utilized pressure data in stochastic estimation procedures. The Shuttle Entry Air Data System (SEADS) program of the 1980's used a flush-mounted air data system to estimate the pressure distribution across the Space Shuttle forebody during entry. The MEDLI program's pressure data system is in large part based on the SEADS concept. The SEADS project was able reconstruct the free-stream conditions during shuttle entry successfully, and verified its results with simulation and wind tunnel data.[23] However, reconstructions based on SEADS data did not blend the inertial measurements with the pressure distribution data. Instead, a sequential batch-filter was used together with a database of pressure distributions on the vehicle forebody for different flight conditions to estimate the aerodynamic parameters that would create the pressure measurements at the transducers during an EDL sequence. As such, potential coupling between uncertainties in the trajectory estimate and uncertainties in the atmosphere estimate were not considered in the SEADS analysis.

Fortunately, MSL will become the first mission to collect a large volume of Mars pressure data during the hypersonic descent phase. Due to the large uncertainty in our knowledge of the Martian atmosphere, a trajectory reconstruction of a Mars EDL sequence that can also estimate the atmospheric profile with a high degree of certainty would be a significant scientific and engineering resource.

C. Mars Science Laboratory

The Mars Science Laboratory is going to be a revolutionary spacecraft in many ways. The payload mass, the altitude of the landing site and the landing accuracy will stretch the limits of planetary entry design.[25] In regards to trajectory and atmospheric reconstruction, MSL will carry a set of instruments that will be able to take in-situ measurements of the pressure and temperature distribution on the aeroshell. The instrumentation is known as MEDLI and will consist of two components: MEADS to take atmospheric measurements and MEDLI Integrated Sensor Plug (MISP) to take aerothermodyamic data.[8]

Particularly, MEADS will provide a data set that will allow the estimation of atmospheric properties without confounding the uncertainties in the knowledge of the aerodynamic coefficients. One of the science objectives of MEADS is to reconstruct atmospheric properties to within certain bounds. Specifically, it is to
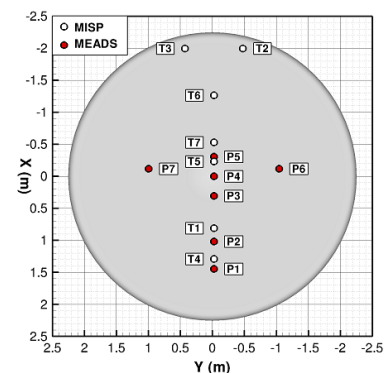

Figure 3. MEDLI sensor locations.[24]

estimate dynamic pressure to within $\pm 2\%$, free-stream Mach number to within $\pm 0.2\%$, and angle of attack and sideslip angle to within $\pm 0.5\%$. In order to achieve these targets, MEADS will collect pressure data from seven pressure transducers located around the forebody of the aeroshell. Figure 3 shows the locations of the pressure transducers as well as the thermocouples that are part of MISP.

The locations of the transducers are based on predicted pressure distributions on the forebody so that there is enough redundancy to reconstruct all of the targeted atmospheric properties. Note that the stagnation pressure is expected to be around transducers P1 and P2 while P6 and P7 serve as the transducers which will help reconstruct the sideslip angle. Although the transducers that will be used for MEADS can sample at high rates, due to memory constraints, both pressure and temperature data will be saved at an effective sampling rate of 8 Hz. However, this will still be higher sampling rate of Martian atmospheric data than any previous mission. This paper will consider the effect of MEADS data on trajectory and atmospheric reconstructions. The reader is referred to the work of Edquist et al.[24] to learn about the effect of MISP data on aerothermodynamic modeling.

III. Deterministic Estimation Procedure

Traditional reconstruction techniques[1–4] have used deterministic methods to estimate a vehicle's trajectory and atmospheric profile. Data sets have contained the acceleration of the center of mass and the Euler angle rates of the vehicle with respect to an inertial reference frame. These acceleration measurements are sensed accelerations ($a_{0,x}$, $a_{0,y}$, and $a_{0,z}$) in the planet-centric coordinate system and the attitude measurements are inertial angular rates (p, q, r) in the vehicle-fixed coordinate system, where x, y, and z-axis refer to North, East, and down directions. To begin the reconstruction, the initial state vector of the vehicle has to also be known. The trajectory state vector consists of position, velocity and attitude of the vehicle. Vehicle position is usually given in terms of the radius to the vehicle from the center of the planet (r) and the vehicle's planet-centric latitude (Φ), and longitude (Θ). Planet-detic latitude can replace planet-centric latitude in the state vector, but proper conversion between the two reference frames should be made.[26] Velocity states (u, v, w) are expressed in the vehicle-fixed reference frame and give the spacecraft's inertial velocity. Attitude is usually described in terms of the aerodynamic Euler angles, namely yaw (ψ), pitch (θ) and roll angles (ϕ). However, the equations of motions involving these Euler angles contain trigonometric functions that approach singularities at certain angle values. In order to avoid this situation, the angles are usually converted into quaternions or Euler parameters (e) that represent the attitude of the body using four normalized parameters. The conversion from Euler angles to Euler parameters is given by Kuipers et al.[27]

After expressing the initial states in terms of the state elements discussed above, the equations of motion can be used to propagate the trajectory from initial time to final time. Equation (1) displays the set of equations of motion expressed in the planet-centric reference frame.[28] The gravitation component of acceleration (g) is dependent on the gravitational model and is usually problem-specific. Normally, a second zonal harmonic model is sufficient for EDL trajectory reconstruction purposes, although higher-fidelity models can be used. Ω is the planet angular velocity.

$$\dot{r} = -w \tag{1a}$$

$$\dot{\Phi} = u/r \tag{1b}$$

$$\dot{\Theta} = v/r \cos \Phi - \Omega \tag{1c}$$

$$\dot{u} = a_{0,x} + (1/r)(uw - v^2 \tan \Phi) + g_x \tag{1d}$$

$$\dot{v} = a_{0,y} + (1/r)(uv \tan \Phi + vw) + g_y \tag{1e}$$

$$\dot{w} = a_{0,z} - (1/r)(u^2 + v^2) + g_z \tag{1f}$$

$$\begin{bmatrix} \dot{e_0} \\ \dot{e_1} \\ \dot{e_2} \\ \dot{e_3} \end{bmatrix} = \frac{1}{2} \begin{bmatrix} -e_1 & -e_2 & -e_3 \\ e_0 & -e_3 & e_2 \\ e_3 & e_0 & -e_1 \\ -e_2 & e_1 & e_0 \end{bmatrix} \begin{bmatrix} p \\ q \\ r \end{bmatrix} \tag{1g}$$

Once the trajectory has been reconstructed, atmospheric parameters can be estimated using the inertial acceleration measurements, knowledge of the aerodynamic coefficients of the vehicle and the velocity history during the descent. Equation (2), which is based on the definition of the axial force coefficient (C_A), shows how the free-stream density (ρ_∞) can be estimated from the sensed axial acceleration ($a_{0,x}$) and the reconstructed velocity (V). Mass (m) of the

vehicle and reference area (S) are also present in the equation.

$$\rho_\infty = \frac{ma_{0,x}}{0.5V_\infty^2 SC_A}$$

(2)

From the density, pressure and temperature profiles can be reconstructed using the hydrostatic equation and the ideal gas equation of state. Both of these equations, however, are only valid within certain assumptions, such as that the atmosphere is in hydrostatic equilibrium and that the atmosphere adheres to the ideal gas law, which neglects the molecular size of the atmospheric components and ignores intermolecular interactions. Equation (3) lists both the hydrostatic equation and the ideal gas equation, where h is altitude (down positive), R is the gas constant for the atmosphere being reconstructed and T is the temperature. The hydrostatic equation is integrated from an initial pressure, which introduces another source of uncertainty that must be accounted for when using deterministic estimation methods.

$$\frac{dP}{dh} = \rho g$$

(3a)

$$T = \frac{P}{\rho R}$$

(3b)

The atmospheric reconstruction procedure described above does not include the uncertainties in the axial force measurements or the aerodynamic coefficients as weighting factors in the estimate of the density. Thus, atmospheric uncertainty and aerodynamic uncertainties are not separable. The uncertainty in the density trickles down to the estimate of the pressure and temperature. However, if additional sensors, such as pressure transducers, can be used to measure pressure distribution around the vehicle during an EDL sequence, the uncertainties in the atmospheric parameters can be quantified independently of the vehicle aerodynamics. This is the motivation behind the inclusion of the MEADS sensors in the upcoming MSL mission. As mentioned earlier, pressure transducer data has been collected during the Viking missions as well as the Shuttle entry air data experiments. However, in both cases, the pressure data is applied in a deterministic procedure to calculate atmospheric properties. The uncertainty in the pressure measurements or the uncertainty in the aerodynamic coefficients are not considered in the estimation procedure. On the other hand, if a statistical estimation method is used to reconstruct the trajectory and atmospheric parameters concurrently, the measurement uncertainties could easily be used as weighting factors in the estimation procedure.

IV. Statistical Estimation Procedure

Accurate estimation for both the trajectory and atmosphere hinges on a procedure to combine information from the various measurement types into a single estimate of the state. Moreover, the estimate should be biased towards measurement types that are more certain; thus, a weighting factor dependent on the data uncertainty needs to be part of the estimation procedure. There are several estimation algorithms available that allow the use of weighting factors to update an estimate based on the measurements collected. The most common type used in navigation and reconstruction-type applications is the extended Kalman filter. A Kalman filter is based on the idea of creating a nominal trajectory and then predicting values of different types of measurements, such as acceleration, throughout the trajectory. The difference between the actual measurements and the predicted measurements is used to update the nominal trajectory. This statistical estimation procedure is composed of two parts:

 i Measurement equations: A method to predict the measurements at a given state
 ii Statistical filter: An algorithm to combine information from various measurement types

A. Measurement Equations

A key requirement for statistical estimation tools such as the Kalman filter is a representation of what the measurements should be at a given state. The actual measurements can then be compared with the predicted measurements, and the state can be appropriately updated. A Kalman filter is based on linear filter theory, so it assumes the measurements are a linear function of the state vector plus a measurement error. If one considers pressure measurements at n different

transducers, the pressure can be expressed as shown in Eq. (4).

$$P_i = f_i(\mathbf{X}) + \epsilon_{\mathbf{i}} \tag{4a}$$

$$\begin{bmatrix} P_1 \\ . \\ P_n \end{bmatrix} = \begin{bmatrix} f_1(\mathbf{X}) \\ . \\ f_n(\mathbf{X}) \end{bmatrix} \begin{bmatrix} \epsilon_1 \\ . \\ \epsilon_n \end{bmatrix} \tag{4b}$$

Here, P_i is the pressure at the i-th orifice, f represents some function of the state vector ($\mathbf{X}$) and ϵ represents the measurement error. The Kalman filter, like many Bayesian statistical estimators, assumes that the measurement error distribution is normal, and the error is an unbiased estimator, i.e. the expectation of the error, $E[\epsilon] = 0$. For most measurement types, f is a non-linear function, but using a first-order Taylor series expansion, Eq. (4) can be linearized about a point (the nominal estimate of the state) as shown in Eq. (5), where $\mathbf{x}$ is the deviation in state from $\bar{\mathbf{X}}$.

$$P_i = f_i(\bar{\mathbf{X}}) + [\partial \mathbf{f}/\partial \mathbf{X}]_{\mathbf{X}=\bar{\mathbf{X}}} \, \mathbf{x} + \epsilon_{\mathbf{i}} \tag{5}$$

A measurement sensitivity (Jacobian) matrix (H), as seen in Eq. (6), can now be defined.

$$H = \begin{bmatrix} \partial f_1/\partial \mathbf{X} \\ . \\ \partial f_n/\partial \mathbf{X} \end{bmatrix}_{\mathbf{X}=\bar{\mathbf{X}}} \tag{6}$$

The measurement sensitivity equations have to be developed for every measurement type included in the estimation process. Christian et al. discusses the development of the sensitivity matrix for accelerometer and radar altimeter measurements.[7] More detailed expressions for the measurement sensitivity equations pertaining to accelerometer and radar measurements can be found in the works of Karlgaard et al.[26] and Jaswinski et al.[29] In the present analysis, only pressure data measurement equations and their sensitivity matrices are discussed.

Moreover, a special modification of the Kalman filter, known as the Kalman-Schmidt filter, will actually estimate the errors in the measurement types. In a Kalman-Schmidt filter, measurement uncertainties such as bias error, scaling factor error etc. become additional parameters that are estimated in the reconstruction process. Jaswinski et al.[29] discusses on this concept. As mentioned earlier, past Mars EDL reconstructions have utilized the Kalman-Schmidt filter methodology. Yet, all of the past works also used the linear Kalman filter equations for the estimating process. So uncertainty propagation in the highly non-linear dynamics of the trajectory and the atmosphere might have been ignored. Thus, in the current analysis, only an extended Kalman filter tool that uses the non-linear equations of motion for state propagation has been used. Kalman-Schmidt filter's capability of measurement error estimation has been reserved for possible future work.

Measurement sensitivity expressions for pressure data are developed by numerical differentiation due to the complexity of the expressions relating the trajectory states with the aerodynamic states. The measurement prediction expressions are functions of the state vector that normally consists of the position, velocity, and attitude of the vehicle. However, for the pressure measurement case, free-stream pressure (p_∞) and free-stream density (ρ_∞) are added to the state vector. Their equations of motion are derived from the hydrostatic equation and an atmospheric equation of state, respectively (Eq. (7)). For this study, the isothermal gas equation of state was used, but any other state equation that takes advantage of a model of the gas dynamics can be substituted.

$$\dot{P}_\infty = \rho_\infty g w \tag{7a}$$

$$\dot{\rho}_\infty = \rho_\infty^2 g w / P_\infty \tag{7b}$$

During the hypersonic phase, the velocity of the vehicle is large with respect to the wind velocity. So the planet-relative velocity can be used to calculate the angle of attack and angle of sideslip (Eq. (8)). The relative velocity to the wind should be used for more precision. In those cases, the wind speed is included as a part of the state vector, but an equation of motion for the wind speed must then be included. For simplicity, winds are not modeled in this study. The two orientation angles can then be combined into a total angle of attack, α_t (also Eq. (8)).

$$\alpha = \tan^{-1}(w/u) \tag{8a}$$

$$\beta = \sin^{-1}(v/V) \tag{8b}$$

$$\alpha_t = \cos^{-1}(\cos\alpha\cos\beta) \tag{8c}$$

The velocity magnitude can be used to calculate the local Mach number. The speed of sound needed for Mach number calculation is a strong function of altitude and can be calculated from the state vector. Finally, the pressure port locations have to be stated. Normally, the locations of these orifices are known in terms of clock (ζ) and cone (η) angles. The cone angle describes the orifice's location with respect to the maximum diameter of the aeroshell. The clock angle describes the port's location on the aeroshell from the y-axis in the y-z plane. Since the pressure ports' orientation with respect to the forebody does not change during the flight, the cone and clock angles are constant throughout the trajectory. Once the total angle of attack, Mach number and the clock and cone angles of the ports are known, the pressure coefficient (C_p) at each orifice can be found from tables created from the vehicle aerodynamic database. An example of such a table is shown in section V. as Table 3. After the pressure coefficient is found, the pressure at each surface location can be calculated using the vehicle velocity and free-stream pressure and density which are state elements. The sensitivity matrix can be calculated by perturbing each of the state elements by a small amount and calculating the change in the predicted port pressure. This numerical method of calculating the sensitivity matrix is necessary since a closed form solution is not possible due to the fact that the pressure coefficient values are being computed from tables. Numerical ill-conditioning issues can arise based on what tolerance value is used to perturb the pressure prediction equations.

B. Extended Kalman Filter

The next step in the reconstruction process is to use a statistical filter to combine the measurement information with the nominal estimate of the state. For this study, this process was achieved using an extended Kalman filter. A Kalman filter is based on linear filter theory and uses the difference between predicted and measured data to update the estimate of the state. An extended Kalman filter is a modification of the original Kalman filter to express the nonlinearity in the system dynamics that is lost in the linearization needed for the original Kalman filter. Consider the linearization of the state vector at time increment k as a function of the state at time k-1 and a random state noise vector ($\mathbf{w}$) as seen in Eq. (9). Recall that $\mathbf{x}$ is the deviation in state and $\mathbf{X}$ is the state vector.

$$\mathbf{X_k} = \mathbf{X_{k-1}} + \left[\frac{\partial \mathbf{X(t_k)}}{\partial \mathbf{X(t_{k-1})}}\right]\mathbf{x_{k-1}} + \mathbf{w} = \mathbf{X_k} + \mathbf{\Phi_k x_{k-1}} + \mathbf{w} \tag{9}$$

The state transition matrix ($\mathbf{\Phi}$) is the function that propagates the state from k-1 to k. The linear Kalman filter needs a nominal trajectory from the initial state to the end state, and the filter estimates the deviation in the state around this nominal trajectory. The extended Kalman filter does not need a nominal trajectory from the start to the end of the trajectory. Instead, the propagation from k-1 to k is done using the nonlinear equations of state. Then, when the state estimate is updated at time k using the measurements, this new estimate is used to propagate to time k+1. Thus, the nonlinearity inherent in the system dynamics can be better handled using the extended Kalman filter algorithm rather than the linearized Kalman filter.

In addition to the equation that defines the state vector, relationships are also needed to define the uncertainty in the state and how these values propagate over time. In Eq. 4, ϵ was introduced as the measurement error. The state vector also has a similar error term known as the state error vector ($\mathbf{e_k}$) which contains the error in each element of the state vector at time k. The EKF assumes that the state error is also normally distributed and thus a state covariance matrix ($\mathbf{P}$) can be introduced which is defined as $\mathrm{E}[\mathbf{e_k e_k^T}]$. A measurement covariance matrix ($\mathbf{R_k}$) can also be defined at time k where $\mathbf{R_k} = \mathrm{E}[\epsilon\epsilon^T]$. As is the case with the state vector, the state covariance vector must be propagated from time k-1 to k. The state transition matrix can be used to accomplish this operation as seen in Eq. (10), where $\mathbf{Q_k}$ is the state noise covariance (i.e. $\mathbf{Q_k} = \mathrm{E}[\mathbf{ww^T}]$).[30]

$$\mathbf{P_k} = \mathbf{\Phi_{k-1} P_{k-1} \Phi_{k-1}^T} + \mathbf{Q_{k-1}} \tag{10}$$

A Riccatti-type differential equation can also be used to update the covariance vector as seen in Eq. (11).[31] Here $\mathbf{A}$ is the Jacobian of the equations of motion with respect to the state vector and produces a matrix similar to what is found in Eq. (6) for the measurement expressions. $\mathbf{B}$ is the partial derivatives of the equations of state with respect to the state noise vector. All of these matrices are evaluated at the current time k-1 and are used to propagate $\mathbf{P}$ to time k.

$$\mathbf{\dot{P}} = \mathbf{AP} + \mathbf{P^T A^T} + \mathbf{BQB^T} \tag{11}$$

In order to begin the EKF process, a nominal estimate at the current time must be found. If the current time is k, then the nominal state estimate ($\mathbf{\bar{X}}_k$) can be found from the final estimate at k-1 as described before. The covariance matrix

can be similarly estimated at time k ($\bar{\mathbf{P}}_k$).Then, the best state estimate at time k ($\hat{\mathbf{X}}_k$) is found by Eq. (12a), where $\mathbf{K_k}$ is the Kalman gain (Eq. (12b)) and $\mathbf{y_k}$ is the measurement residual vector. The measurement residual vector ($\mathbf{y}$) is defined as the difference between all of the actual measurements at the current time and the corresponding predicted measurements at the nominal state. Within the expression for the Kalman gain, H_k is the measurement sensitivity matrix and evaluated at time k. Finally, the state covariance for the best estimate ($\hat{\mathbf{P}}_k$) is found using Eq. (12c), where I is the identity matrix.

$$\hat{\mathbf{X}}_{\mathbf{k}} = \bar{\mathbf{X}}_{\mathbf{k}} + \mathbf{K_k y_k} \tag{12a}$$

$$K_k = \bar{\mathbf{P}}_{\mathbf{k}} \mathbf{H_k^T} \left(\mathbf{H_k} \bar{\mathbf{P}}_{\mathbf{k}} \mathbf{H_k^T} + \mathbf{R_k} \right)^{-1} \tag{12b}$$

$$\hat{\mathbf{P}}_{\mathbf{k}} = (I - K_k H_K) \bar{\mathbf{P}}_{\mathbf{k}} (\mathbf{I} - \mathbf{K_k H_k})^{\mathbf{T}} + \mathbf{K_k R_k K_k^T} \tag{12c}$$

The algorithm for this filter can be summarized as follows:

1. Initialize the state vector and the state covariance matrix at time t_k-1 = t_0 and let k = 1, where k is an index of the epoch when measurement was taken.
2. Read in measurement at time t_k.
3. Calculate a nominal state at t_k ($\bar{\mathbf{X}}_k$) by integrating the non-linear equations of motions (Eqs. (1) and (7)) with $\hat{\mathbf{X}}_{k-1}$ as the initial condition.
4. Calculate the nominal state covariance matrix ($\bar{\mathbf{P}}_k$) using the state transition matrix (Eq. (10)) or the Riccati equations (Eq. (11)).
5. Calculate the measurement residual vector ($\mathbf{y_k}$), the measurement sensitivity matrix (H_k), and the Kalman gain (K_k) using the nominal state and state covariance (Eq. (12b)).
6. Calculate the best estimate of the state ($\hat{\mathbf{X}}_k$) and state covariance ($\hat{\mathbf{P}}_k$) using Eqs. (12a) and (12c).
7. Increment counter k and go back to step 2 until measurements at all times have been read.

A difference between the extended Kalman filter and the standard Kalman filter is highlighted in step 3 of the algorithm where the nominal state is calculated by integrating the non-linear equations and the last best estimate is used as the initial condition. In a highly non-linear problem, large deviations could be propagated through a linear approximation of the equations of motion. The extended Kalman filter effectively re-linearizes the state estimate at the last best estimate found whenever a new measurement is processed, thus reducing deviations that can result from linearizing a non-linear problem.

An advantage of the extended Kalman filter is that it provides an efficient way to incorporate more than one type of measurement. Each measurement type has a unique measurement sensitivity matrix and observation covariance. Thus, when the filter is processing measurement type A, the appropriate H and $\mathbf{R}$ matrices are used with the nominal state error covariance. If measurement type B has to be processed at the next time step, only the H and $\mathbf{R}$ matrices will change in the algorithm.

Moreover, one can see that the state is affected by three factors by looking at Eq. (12b) for the Kalman gain and Eq. (12a) for the state update. The Kalman gain is a function of the current state uncertainty ($\mathbf{P_k}$), the measurement uncertainty ($\mathbf{R_k}$) and the residual between the predicted and actual measurements ($\mathbf{y}$). If the state estimate is more certain than the measurements being processed, the filter will be minimally affected by the data.

In addition, the filter can blend the information from the various data types, and the state estimate will be weighted towards the measurement with the smallest observation error, which can be gleaned from its observation covariance matrix. When two or more data types are being processed sequentially, the state estimate initially may oscillate between the measurements from the differing sources, but the filter quickly uses the weighting information from the R matrices to calculate the blended estimate.

Finally, the residual of the measurements can scale the update of the state. If the predicted measurements were very close to the actual measurements, then the state update will be minimal. To demonstrate this concept, Mars Pathfinder reconstruction data is used below. Details about this trajectory reconstruction can be found in the work of Christian et al,[7] with additional background information in Spencer et al.[1] Figure 4 demonstrates the effect of data blending by showing the estimate of altitude for Mars Pathfinder when the radar altimeter measurements are included with the accelerometer measurements. One way to compare the effect of uncertainty in the estimate is to vary the weighting factor for the measurements being used. As one can see, the altitude estimate initially oscillates between the accelerometer and radar altimeter observations, but finally the EKF moves the estimate towards the less uncertain measurements, which in this case comes from the radar altimeter. Another advantage of the extended Kalman
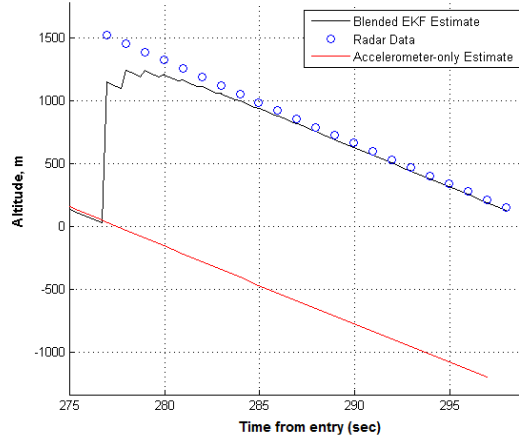
Figure 4. Effect of blending different data types on the estimate of altitude for Mars Pathfinder. The altitude shown is above Mars mean radius.

filter is that it can be used to sequentially reconstruct the trajectory in either a forward or backwards manner. The reconstruction can be conducted starting from the atmospheric entry all the way down to the ground (forward pass) or using a projected landing location to estimate the trajectory up to the entry conditions (backwards pass). The forward pass starts its estimate from an initial state and covariance that is found independent of the trajectory reconstruction process. Also, the reconstruction is conducted in a chronological manner. The backwards pass has the advantage of starting at a smaller uncertainty value as it begins from the end of the forward estimate. The forward (f) and backward (b) pass estimates can be combined using the Fraser-Potter smoothing solution[32], which is shown in Eqs. (13).

$$\hat{\mathbf{P}}_{\mathbf{k}} = \left[\hat{\mathbf{P}}_{\mathbf{f,k}}^{-1} + \hat{\mathbf{P}}_{\mathbf{b,k}}^{-1}\right]^{-1} \tag{13a}$$

$$\hat{\mathbf{X}}_{\mathbf{k}} = \hat{\mathbf{P}}_{\mathbf{k}}\left[\hat{\mathbf{P}}_{\mathbf{f,k}}^{-1}\hat{\mathbf{X}}_{\mathbf{f,k}} + \hat{\mathbf{P}}_{\mathbf{b,k}}^{-1}\hat{\mathbf{X}}_{\mathbf{b,k}}\right] \tag{13b}$$

An advantage of combining both the forward and backward estimates is to find an optimal estimate of the trajectory. The forward pass estimate at time k uses the measurement data from entry to k, while the backward pass uses the measurement data from landing time to k. The combined smoothed estimate can use measurement data at all times to create the estimate at k. Figure 5 shows the forward, backward, and smoothed estimate of the altitude of Mars Pathfinder, which is used to demonstrate the advantage of the smoothing algorithm. The one-sigma uncertainties associated with the three estimates are also shown.

V.   Test Case

Results from a sample case are presented in this section to test the methodology. As MSL will not provide a data set until 2012, measurements from a ballistic range test of two Crew Exploration Vehicle (CEV) models are used to apply the trajectory and atmospheric reconstruction procedures.[33] The ballistic range test was conducted on July 15, 2008 at the Aberdeen Army Proving Ground (APG) in Aberdeen, MD. As shown in Figure 6, the test utilized two titanium models of the CEV. The models were referred to as the pressure-telemetry modules (PTM). The PTMs were launched from a ballistics range gun and data was collected for approximately 20 seconds after they exited the muzzle. Although data sets for both models were available, since both models followed similar trajectories, only the results for the second model (labeled PTM2) are analyzed below. Some key parameters for PTM2 are also summarized in Figure 6. The center of gravity (CG) locations are with respect to U.S. Army Research Laboratory coordinate system convention.

As can be surmised from the name of the experiment, the models collected pressure data along with telemetry data during their flight. The telemetry information consisted of sensed accelerations, angular rates and magnetometer measurements. Additionally, a tracking radar calculated the range and range rate of the models with respect to a fixed station. Also, the on-site meteorological station provided temperature, pressure and wind speed information.
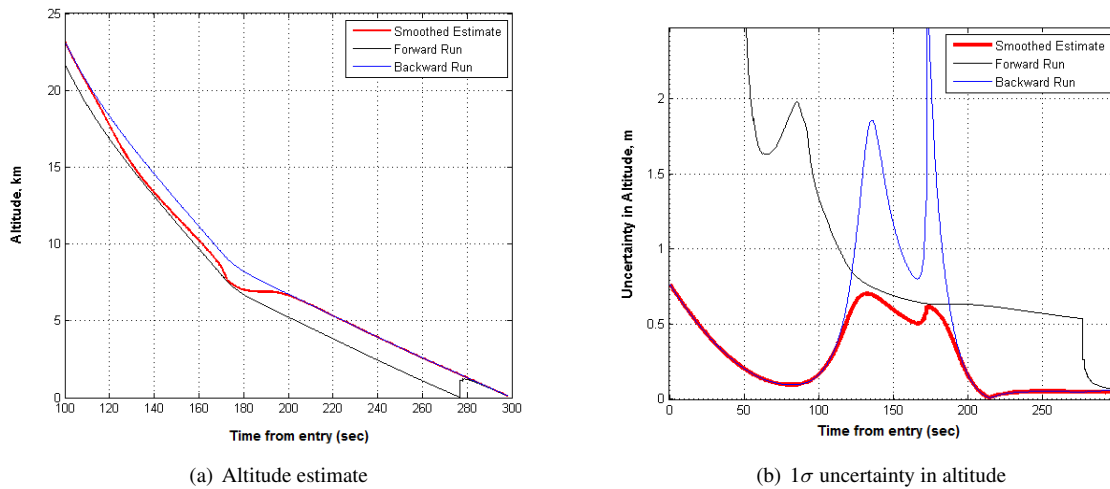
(a) Altitude estimate

(b) 1σ uncertainty in altitude

Figure 5. Forward and backward runs and smoothing on the estimate of altitude for Mars Pathfinder.

Mass	18.422	lb
CG_x	2.488	in
CG_y	0.002	in
CG_z	0.187	in
I_{xx}	69.144	lb-in^2
I_{yy}	50.978	lb-in^2
I_{zz}	51.322	lb-in^2
Length	4.268	in
Diameter	6.500	in
Data sampling rate	7.940	KHz

Figure 6. CEV model (PTM2)used in the pressure-telemetry tests. [33]

There are fundamental differences between MSL and this ballistic range test. The ballistic range model achieves a maximum Mach number of 3.5 during its flight, while MSL is going to achieve speeds several times greater. The PTM only climbs up to 800 meters; thus, the data set will not contain measurements from the upper atmosphere, which can compare well with the thin atmosphere of Mars. Finally, since the PTM is shot out of a gun, it is acted upon by very high accelerations and angular rates at the beginning of the flight. These accelerations are illustrated in Figure 7.

As one can see from the figure, the vehicle undergoes almost 7000 g's of acceleration and several hundred degrees per second of angular velocity. MSL will not face this type of flight regime. However, despite these differences, the EKF algorithm should be insensitive to the magnitude of data that it handles. Regardless of the actual values of the data, if the measurement equations and the algorithm are simulated correctly and proper values are used for the observation errors, the filter should be able to reconstruct the trajectory and atmosphere that the PTM encounters. Furthermore, since the types of observations that the PTMs obtained are comparable to the types of data MSL is planning to obtain, a successful reconstruction of the PTM's trajectory bodes well for similar success with MSL's data set.

As mentioned in section IV.B., the pressure measurement prediction equations are dependent on tabulated values of the pressure coefficient as function of total angle of attack, Mach number, and the orifice cone and clock angle. An example of such a table for PTM2 is given in Table 3.

To match data types with MSL, this analysis only considered the acceleration, angular rates, radar measurements and pressure observations from the PTM2 data set. As was shown in Eq. (1), accelerations and angular rate information are used in the equations of motion to propagate the state from one time increment to another. So these measurement types are not explicitly used in the EKF tool using Eq. (12). However, the state noise vector ($\mathbf{w}$) is defined based on the measurement error of the accelerometer and gyroscopes, thus the uncertainty in these data appears implicitly in

(a) Axial acceleration for PTM2
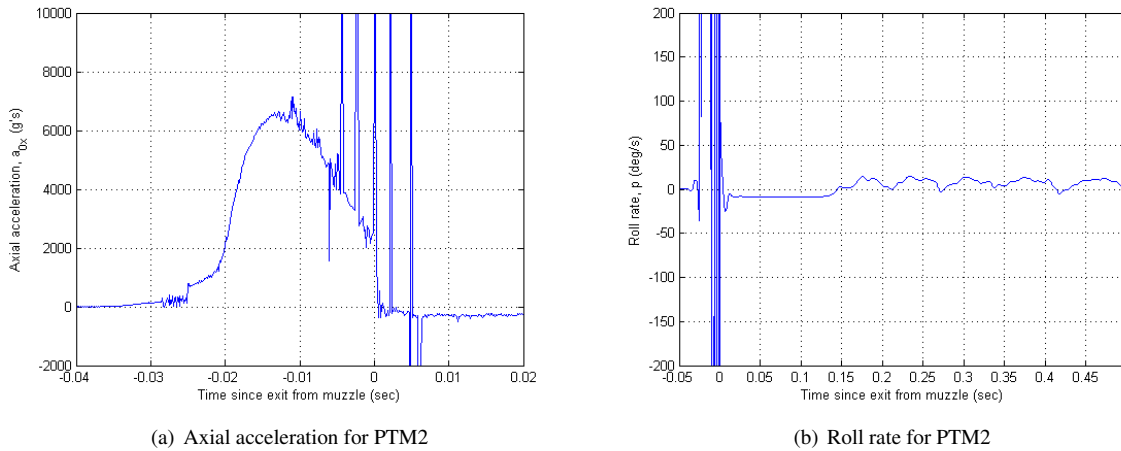

(b) Roll rate for PTM2

Figure 7. Example of inertial measurement unit observations for PTM2.

Table 3. Pressure coefficient values for PTM2 at M = 0.6 and η = 14 degrees.

Angle of attack, α (deg.)	Clock Angle, ζ (degrees)					
	0	5	10	15	20	25
0	1.096745	1.096747	1.096749	1.09675	1.096752	1.096754
5	1.096761	1.096763	1.096764	1.096766	1.096768	1.096770
10	1.096772	1.096774	1.096776	1.096778	1.096779	1.096781
15	1.096780	1.096781	1.096783	1.096785	1.096786	1.096788
20	1.096783	1.096784	1.096786	1.096788	1.096789	1.096791
25	1.096781	1.096783	1.096784	1.096786	1.096788	1.096789
30	1.096775	1.096777	1.096778	1.096780	1.096782	1.096783
35	1.096765	1.096767	1.096768	1.096770	1.096771	1.096773
40	1.096750	1.096752	1.096753	1.096755	1.096756	1.096758
45	1.096731	1.096733	1.096734	1.096736	1.096737	1.096739

the EKF through the state noise covariance matrix, **Q**. The pressure measurements were taken at five port locations on the forebody of the vehicle. Figure 8 shows the locations of the ports on the forebody of the vehicle and pressure data from those ports during the trajectory. Figure 9 displays the range data from the tracking radar. The instruments and
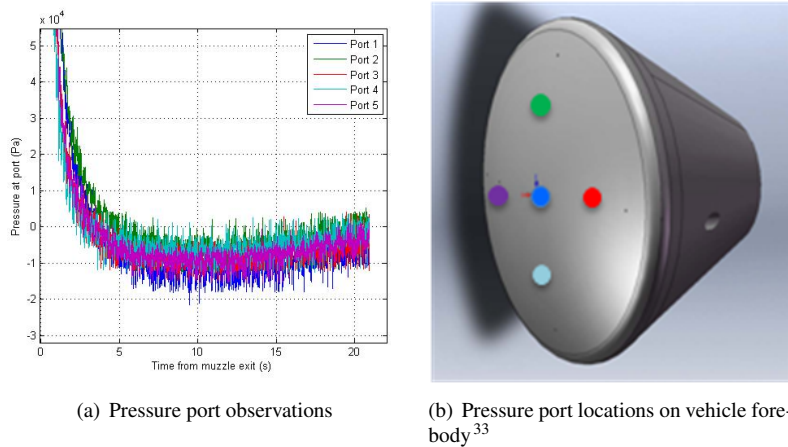

(a) Pressure port observations

(b) Pressure port locations on vehicle forebody[33]

Figure 8. Pressure port locations and observations for PTM2.

(a) Range from radar station

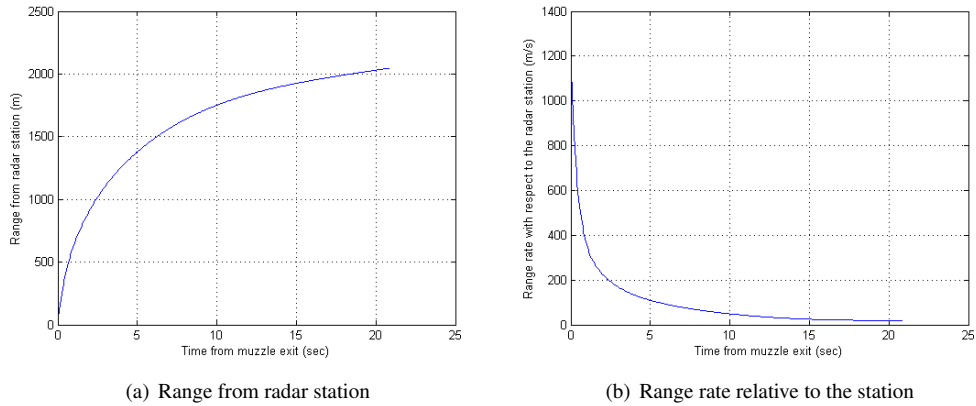(b) Range rate relative to the station

Figure 9. Tracking radar observations for PTM2.

their measurement errors are summarized in Table 4. The measurements errors reported in the table are the 1σ values and the errors are assumed to be normally distributed with an expectation of zero.

Table 4. Measurement uncertainties of sensors on PTM2.

Observation	Sensor Model	1σ uncertainty
Accelerometers	ADXL-78	0.0686 m/s
Angular rates	ADXRS300	0.025 deg/s
Pressure transducers	XCEL-100-500A	5 psi
Radar position	APG tracking radar	
Distance		1 m
Angles		0.1146 deg.
Radar rate	APG tracking radar	
Rate		1 m/s
Angular rate		0.1 deg/s

As can be surmised from Fig. 7, the initial state of the vehicle at the muzzle exit was hard to assess due to the high acceleration and angular rates encountered by model in the gun. The initial state inside the gun was known, but since the pressure and radar measurements are only taken once the vehicle exits the gun, the initial state for the EKF had to be that point. Thus, using only the accelerometer and angular rate measurements, the state vector at 0.001 seconds past the muzzle exit is determined. This data serves as the initial state for the EKF and is summarized in Table 5. However, since the accelerations and angular rates are so high and the sensors reach saturation at several points, very high values are assigned for the initial state uncertainties. As a result, the forward run of the EKF will be initially more sensitive towards the measurements in updating the states. Note that this aspect of analyzing the PTM data is quite different from what would occur with a Mars data set. The initial state for Mars EDL systems are found from the end state of the navigation orbital determination (OD) solutions, which provide the state vector with high accuracy. Thus, for a Mars reconstruction, the EKF will start from a relatively certain initial state. The smoothed best estimate for PTM2's trajectory and the atmosphere it encountered is given below. The altitude and Mach number history of the model is seen in Figure 10.

The altitude and Mach number history compare well with simulated results for the test. The figures above also show that the uncertainty in the estimate is small. Although the initial state uncertainties were set to be large numbers, after the forward and backward run and the smoothing procedure, the uncertainty in the state estimates decrease dramatically. Additionally, as was discussed before, the goal of an atmospheric reconstruction is to determine the free-stream pressure and density profile seen by the vehicle during its trajectory. However, since this vehicle only reached about 800 meters, the change in pressure and density was not large. Nevertheless, the reconstructed values for pressure are compared with the data collected by the ballistic range's meteorological station in Fig. 11. Density data was not given by the meteorological station, and thus it is not shown here. However, the change in density was also just as small as the change in pressure.

Table 5. Initial state vector used for PTM2.

t_0	0.001 sec
u	-912.628 m/s
v	25.475 m/s
w	-193.985 m/s
h	2.43 m
Φ	39.466 deg.
Θ	283.830 deg.
ψ	195.743 deg.
θ	11.485 deg.
ϕ	-2.387 deg.
P_∞	101.783 kPa
ρ_∞	1.1807 kg/m^3

(a) Estimated altitude

(b) Estimated Mach number
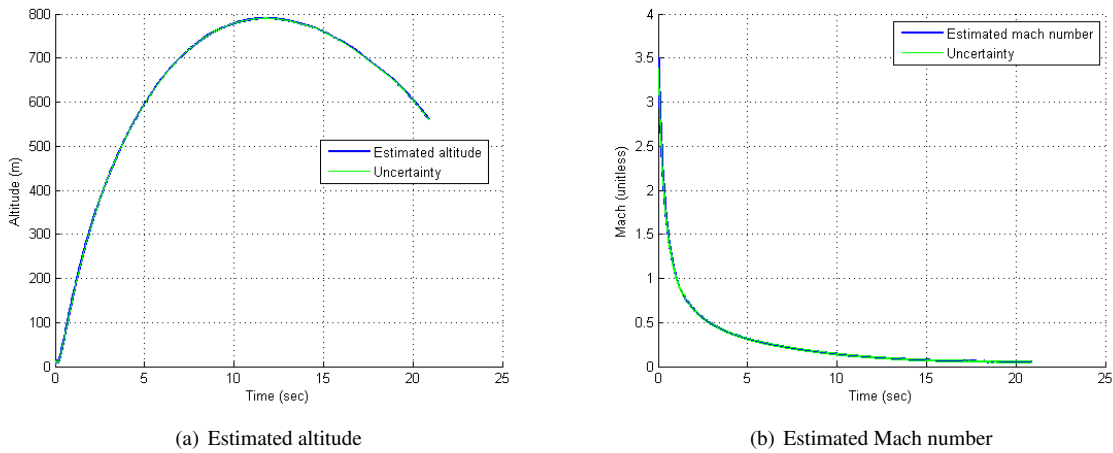
Figure 10. Reconstructed altitude and Mach number history of PTM2 and 1σ uncertainty in the estimate.
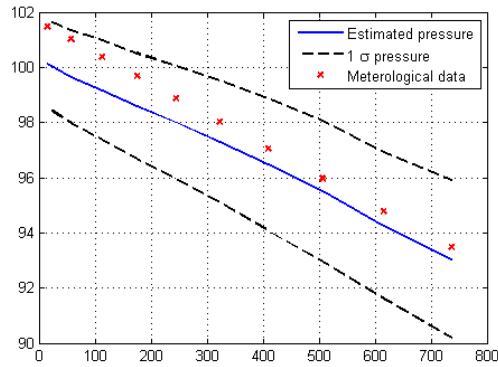
Figure 11. Reconstructed pressure estimate for PTM2.

Recall that the meteorological data was not included in the EKF process. The free-stream conditions shown in the figure are a result of only inertial measurements, radar measurements and the on-board pressure observations. The fact that it agrees very well with an independent source of pressure observations demonstrates the strength of the reconstruction methodology. Besides free-stream conditions, another objective of MSL's MEDLI program is to determine the orientation angles of the vehicle during entry, descent and landing. As has been shown before, angle

of attack and sideslip angle affect the pressure distribution on the vehicle forebody, and thus if these values can be reconstructed, then there will be additional insight towards the vehicle's interaction with the atmosphere. The estimated angle of attack and sideslip angle history for PTM2 are shown in Fig. 12.
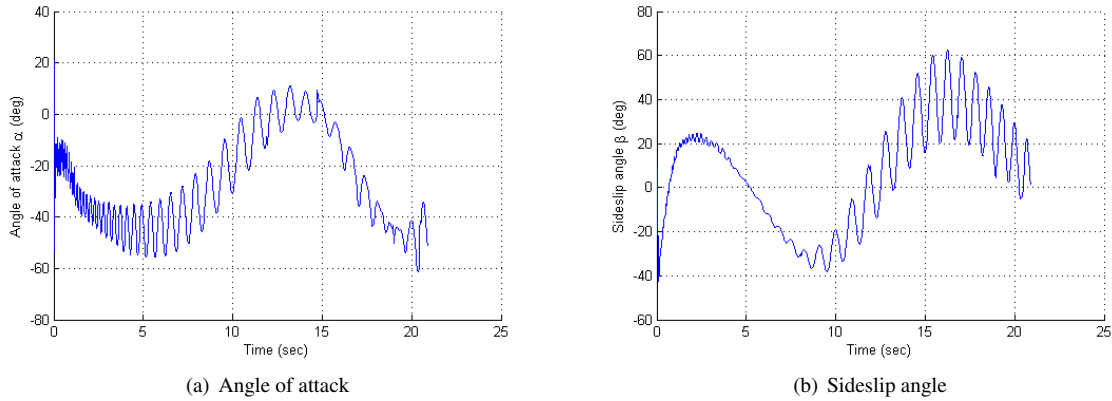

(a) Angle of attack

(b) Sideslip angle

Figure 12. Reconstructed angle of attack and sideslip angle of PTM2.

Unlike the free-stream pressure estimate there were not any independent observations to compare with the reconstruction of the orientation angles. However, the reconstructed values compared favorably with what was predicted pre-flight. The high accelerations and angular rates experienced by the model (Figure 7) when launched from the gun still have an effect on the reconstruction estimate. The angle of attack and sideslip angles experience significant oscillation in the first one second of flight and this is apparent from looking at the above figures. However, when the high accelerations dissipate with time, the orientation angles are reconstructed without significant noise. This last observation bodes well for MSL reconstruction as that vehicle will not face the high accelerations and rates seen by PTM2.

Since the ballistic range data does not have any truth data with which the reconstructed parameters can be compared, simulated data was created to additionally verify the methodology. The tool was tested with a data set created from a simulated trajectory that the ballistic range models were expected to take during their flights. The measurement equations for accelerometer, gyro, radar altimeter and pressure transducers described in Section IV. A. were used to construct the data. Then noise was applied on the data based on a Gaussian distribution with a mean of zero and variance determined from the sensor uncertainties (Table 4). Figure 13 shows the reconstructed altitude and Mach number which demonstrates the capability of the tool to reconstruct trajectory parameters (such as altitude) and atmospheric values (such as Mach number). As can be seen in the figure, the actual data and the reconstructed parameters fall very close to each other and are within the 1σ uncertainty bounds.
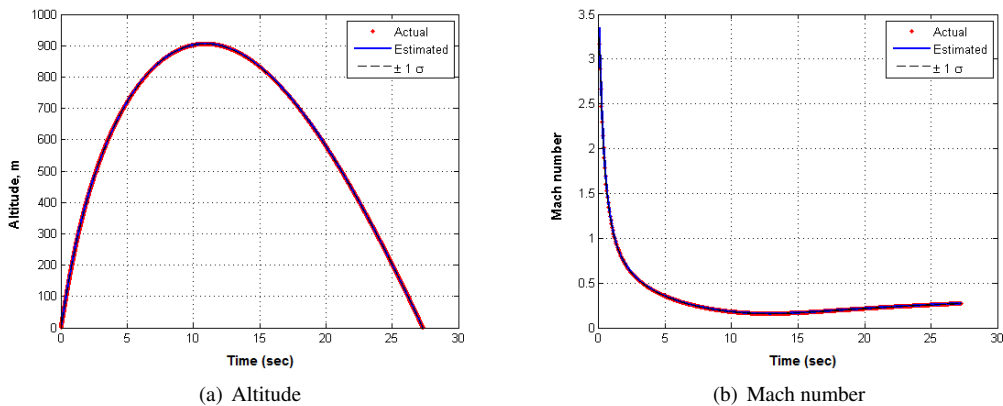

(a) Altitude

(b) Mach number

Figure 13. Actual and reconstructed trajectory and atmospheric parameters based on a simulated ballistic range data set.

VI.   Conclusion

This paper provides a framework on how to use flight data from an entry, descent, and landing sequence to reconstruct the vehicle's trajectory and atmosphere as well as compute the associated uncertainties in these estimates. Past Mars missions have flown limited instrumentation, such as accelerometers, gyroscopes, and radar altimeters that do not provide measurements directly related to the free-stream conditions. Thus, uncertainties in the atmospheric conditions and aerodynamic database knowledge could not be separated. These previous reconstructions have also relied on a deterministic process where the uncertainties of the measurements were not included directly in the estimation and potential coupling between uncertainties in the trajectory and uncertainties in the atmosphere were not estimated. As the upcoming MSL mission will provide forebody pressure measurements during entry together with accelerometer, gyroscope, and radar altimeter data, the Mars EDL reconstruction process can be significantly improved. In this investigation, a statistical reconstruction procedure based on extended Kalman filter theory was developed to take advantage of this new data type. A sample data set from ballistic range tests of a Crew Exploration Vehicle model was used to show results from applying the methodology. The reconstruction method was able to estimate the states of the CEV model well during its twenty second flight. Moreover, the atmospheric conditions that were reconstructed matched well with the meteorological information and pre-flight predictions. The success of the using the reconstruction methodology on this CEV ground-based test data set demonstrates that the trajectory and atmospheric estimation procedure can be successful in the reconstruction effort for MSL.

VII.   Future Work

The results from the test case showed that the proposed method in this paper can be used to estimate trajectory and atmospheric conditions from a data set that contains measurements from an inertial measurement unit, radar altimeter and pressure transducers. However, future work must be done to verify this method using sources other than the data from CEV ballistic range test. Specifically, a MSL simulated trajectory can be used to generate pressure and IMU measurements, and noise can be added to simulate the uncertainty in the measurement values. Then the filter can reconstruct the necessary parameters from this simulated data set. Although this technique is similar to the simulated data of the ballistic range test used to initially verify the reconstruction tool (as seen in Section V.), the MSL simulated data will be similar in its chronology of events to the data expected from MEDLI, and thus the tool could be tested to see if it can meet the science objectives of MEADS. Additionally, the tool and technique can also be modified to include a Kalman-Schmidt filter-like capability to estimate the uncertainties in measurements. As explained earlier, a Kalman-Schmidt filter is able to estimate the different biases and errors in the measurements itself, and with a similar technique one may also estimate the uncertainties in the aerodynamic coefficients while reconstructing the atmosphere and the trajectory. However, this is not simple since the form or model used to describe the aerodynamic coefficient uncertainty still has to be determined. Finally, another addition to the reconstruction work will be to use the estimated uncertainties in trajectory parameters and quantify the margins required in the design of a Mars EDL vehicle. Such a technique will drastically reduce the uncertainties in design as well as increase the capabilities of current EDL vehicles.

Acknowledgments

References

[1]Spencer, D., Blanchard, R., Braun, R., Kallemeyn, P., and Thurman, S., "Mars Pathfinder Entry, Descent, and Landing Reconstruction," *Journal of Spacecraft and Rockets*, Vol. 36, No. 3, 1999, pp. 357–366.

[2]Blanchard, R., "Entry Descent and Landing Trajectory and Atmosphere Reconstruction for the Mars Exploration Rovers Missions A and B," Tech. rep., White paper performed under NASA-JPL subcontract CCNS20568F, The George Washington University, 2008.

[3]Desai, P., Prince, J., Queen, E., Cruz, J., and Grover, M., "Entry, Descent, and Landing Performance of the Mars Phoenix Lander," *AIAA/AAS Astrodynamics Specialist Conference and Exhibit, Honolulu, HI*, No. AIAA 2008-7346, 2008.

[4]Ingoldby, R., Michel, F., Flaherty, T.M., D., M.G., Preston, B., Villyard, K., and Steele, R., "Entry Data Analysis for Viking Landers 1 and 2," Tech. rep., NASA CR-159388, Martin Marietta Corporation, Denver Division, 1976.

[5]Edquist, K. T., "Computations of Viking Lander Capsule Hypersonic Aerodynamics with Comparisons to Ground and Flight Data," *AIAA Atmospheric Flight Mechanics Conference and Exhibit, Keystone, CO*, No. AIAA 2006-6137, 2006.

[6]Desai, P. N. and Knocke, P. C., "Mars Exploration Rovers Entry, Descent, and Landing Trajectory Analysis," *AIAA/AAS Astrodynamics Specialist Conference and Exhibit, Providence, RI*, No. AIAA 2004-5092, 2004.

[7]Christian, J., Verges, A., and Braun, R., "Statistical Reconstruction of Mars Entry, Descent, and Landing Trajectories and Atmospheric Profiles," *AIAA SPACE Conference and Exposition, Long Beach, CA*, No. AIAA 2007-6192, 2007.

[8]Gazarik, M., Wright, M., Little, A., Cheatwood, F., Herath, J., Munk, M., Novak, J., and Martinez, E., "Overview of the MEDLI Project," *IEEE Aerospace Conference, Big Sky, MT*, No. IEEEAC paper No. 1510, 2008.

[9]Desai, P. N., Schoenenberger, M., and Cheatwood, F., "Mars Exploration Rover Six-Degree-of-Freedom Entry Trajectory Analysis," *Journal of Spacecraft and Rockets*, Vol. 43, No. 5, 2006, pp. 1019–1025.

[10]Prince, J. L., Desai, P. N., Queen, E. M., and Grover, M. R., "Mars Phoenix Entry, Descent, and Landing Simulation Design and Modeling Analysis," *AIAA/AAS Astrodynamics Specialist Conference and Exhibit, Honolulu, HI*, No. AIAA 2008-7507, 2008.

[11]Striepe, S., Way, D., Dwyer, A., and Balaram, J., "Mars Science Laboratory Simulations for Entry, Descent, and Landing," *Journal of Spacecraft and Rockets*, Vol. 43, No. 2, 2006, pp. 311–323.

[12]Edquist, K. T., Desai, P. N., and Schoenenberger, M., "Aerodynamics for the Mars Phoenix Entry Capsule," *AIAA/AAS Astrodynamics Specialist Conference and Exhibit, Honolulu, HI*, No. AIAA 2008-7219, 2008.

[13]Euler, E., Adams, G., and Hopper, F., "Design and Reconstruction of the Viking Lander Descent Trajectories," *Journal of Guidance and Control*, Vol. 1, No. 5, 1978, pp. 372–378.

[14]J. T. Schofield, J. R. Barnes, D. C. R. M. H. S. L. J. A. M. J. R. M. A. S. G. W., "The Mars Pathfinder Atmospheric Structure Investigation/Meteorology (ASI/MET) Experiment," *Science*, Vol. 278, No. 5344, 1997, pp. 1752–1758.

[15]Milos, F. S., Chen, Y., Congdon, W. M., and Thornton, J. M., "Mars Pathfinder Entry Temperature Data, Aerothermal Heating, and Heatshield Material Response," *Journal of Spacecraft and Rockets*, Vol. 36, No. 3, 1999, pp. 380–391.

[16]Withers, P. and Smith, M. D., "Atmospheric entry profiles from the Mars Exploration Rovers Spirit and Opportunity," *Icarus*, Vol. 185, 2006, pp. 133–142.

[17]Blanchard, R., "Mars Phoenix Mission Entry, Descent, and Landing Trajectory and Atmosphere Reconstruction," Tech. rep., Work performed under Grant Award No. CCLS20458F, The George Washington University, 2009.

[18]Regan, F. J. and Anandakrishnan, S. M., *Dynamics of Atmospheric Re-Entry*, American Institute of Aeronautics and Astronautics, Inc., Reston, VA, 1993.

[19]Mulder, J., Chu, Q., Sridhar, J., Breeman, J., and Laban, M., "Non-linear aircraft flight path reconstruction review and new advances," *Progress in Aerospace Sciences*, Vol. 35, 1999, pp. 673–726.

[20]Seiff, A. and Jr., D. R., "Use of Entry Vehicle Response to Define the Properties of the Mars Atmosphere," *American Astronautical Society Symposium on Unmanned Exploration of the Solar System, Denver CO*, No. NASA-TM-X-56125, 1965.

[21]Hopper, F., "Trajectory, Atmosphere, and Wind Reconstruction from Viking Measurements," *AIAA/AAS Astrodynamics Conference, Nassau, Bahamas*, No. AAS Paper No. 75-068, 1975.

[22]Blanchard, R. and Walberg, G., "Determination of the Hypersonic-Continuum/Rarefied-Flow Drag Coefficient of the Viking Lander Capsule 1 Aeroshell from Flight Data," Tech. Rep. NASA TP 1793, NASA Report, 1980.

[23]Pruett, C.D., W. H. H. M. and Siemers, P., "Innovative Air Data System for the Space Shuttle Orbiter," *Journal of Spacecraft and Rockets*, Vol. 20, No. 1, 1983, pp. 61–69.

[24]Edquist, K. T., Dyakonov, A. A., Wright, M. J., and Tang, C. Y., "Aerothermodynamic Design of the Mars Science Laboratory Heatshield," *41st AIAA Thermophysics Conference, San Antonio, TX*, No. AIAA 2009-4075, 2009.

[25]Braun, R. D. and Manning, R. M., "Mars Exploration Entry, Descent, and Landing Challenges," *Journal of Spacecraft and Rockets*, Vol. 44, No. 2, 2007, pp. 310–323.

[26]Karlgaard, C., Tartabini, P., Blanchard, R., Kirsch, M., and Toniolo, M., "Hyper-X Post-Flight-Trajectory Reconstruction," *Journal of Spacecraft and Rockets*, Vol. 43, No. 1, 2006, pp. 105–115.

[27]Kuipers, J., *Quaternions and Rotation Sequences*, Princeton University Press, Princeton, NJ, 1999.

[28]Etkin, B., *Dynamics of Atmospheric Flight*, Dover Publications, Inc., Mineola, NY, 2000.

[29]Jaswinski, A., *Stochastic Processes and Filtering Theory*, Academic Press, San Diego, CA, 1970.

[30]Tapley, B.D., S. B. and Born, G., *Statistical Orbit Determination*, Elsevier Academic Press, Burlington, MA, 2004.

[31]Zarchan, P. and Musoff, H., *Fundamental of Kalman Filtering, A Practical Approach*, American Institute of Aeronautics and Astronautics, Inc., Reston, VA, 2000.

[32]Fraser, D. and Potter, J., "The Optimum Linear Smoothers as a Combination of Two Optimum Linear Filters," *IEEE Transactions on Automatic Control*, Vol. 14, No. 8, 1969, pp. 387–390.

[33]Topper, B., "NASA Orion Crew Exploration Vehicle-Pressure Telemetry Module (CEV-PTM) Free Flight Ballistic Range Experiment Performed at APG, MD on July 15, 2008," Tech. rep., US Army Research Laboratory internal document, AMSRD-ARL-WM-BA, Aberdeen, MD, 2008.